Dynamic Modulation of Ionic and Electronic Pathways in Flexible SnS_2-Based Interdigitated Solid-State Supercapacitors

Premkumar Jayaraman, [a,b,c] Hamed Pourzolfaghar, [b,c] Yuan-Yao Li [* b,c] and Helen Annal Therese [* a]

[a] Futuristic Energy Storage Technology Lab (FESTL), Department of Chemistry, Faculty of Engineering and Technology, SRM Institute of Science and Technology, Kattankulathur - 603203, Chengalpattu Dt, Tamil Nadu, India

[b] Department of Chemical Engineering, National Chung Cheng University, Chia-Yi 62102, Taiwan.

[c] Advanced Institute of Manufacturing with High-Tech Innovations, National Chung Cheng University, Chia-Yi 62102, Taiwan.

***** Corresponding author; E-mail address -helena@srmist.edu.in; chmyyl@ccu.edu.tw

Synthesis of tin disulfide (SnS_2)

To synthesize the compound, 24 mg of tin tetrachloride ($SnCl_4 \cdot 5H_2O$) was first dissolved in 2 mL of concentrated HCl, followed by the addition of 30 mL of distilled water. Thereafter, 7.43 mg of thioacetamide (C_2H_5NS) was introduced, and the mixture was stirred for 5 hours until it developed a yellow color. The yellow precipitate was then washed with distilled water and absolute ethanol, filtered, and dried in a vacuum oven at 70°C overnight.

Physical and Chemical Characterizations

Core-level XPS spectra for tin and sulfur were analyzed using CasaXPS for peak fitting. The characteristic Sn $3d_{3/2}$ and Sn $3d_{5/2}$ peaks indicate the presence of both Sn^{2+} and Sn^{4+} oxidation states. Peaks at binding energies of 495.39 and 486.92 eV correspond Sn^{4+}, confirming that the thin film is predominantly composed of SnS_2. Additionally, shoulder peaks at 494.69 eV and 485.78 eV (Energy difference ≈ 8.47eV) indicate a minor fraction of Sn^{2+}, consistent with SnS. For sulfur, the S 2p peaks at 164.00 eV and 162.25 eV correspond to S-Sn^{2+} and S-Sn^{4+} bonds, respectively. The observed 1.75 eV energy differences suggest a significant density of defects within the SnS_2 film. To determine surface stoichiometry, XPS analysis was performed using the *Relative Sensitivity Factor (RSF)* method:

$$Atomic\ \%\ X\ = \left(\frac{\frac{I_X}{RSF_X}}{\sum \frac{I_X}{RSF_X}} \right) \quad \text{(S1)}$$

Where, I_X means Peak area of element (X= Sn, S), RSF_X means Sensitivity factor.

For Tin (Sn): RSF value = 0.974 and Area = 3205 found from XPS. For Sulfur (S): RSF value = 0.935 and Area = 6264 found from XPS.

Using these values, the calculated atomic composition is: Sn (32.93 %) and S (67.07 %). This corresponds to a stoichiometric ratio of Sn:S ≈ 1:2.04, which is consistent with SnS_2.

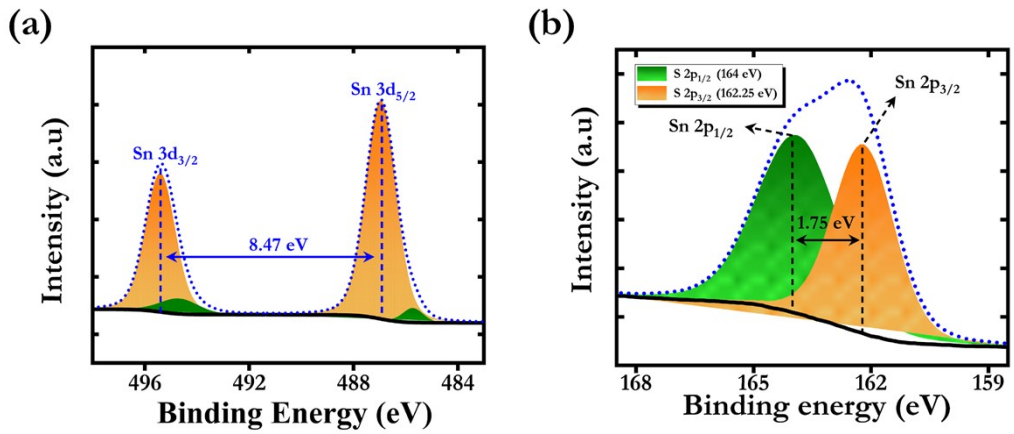

Fig. S1 (a and b) Core level spectrum for Sn and S, respectively.

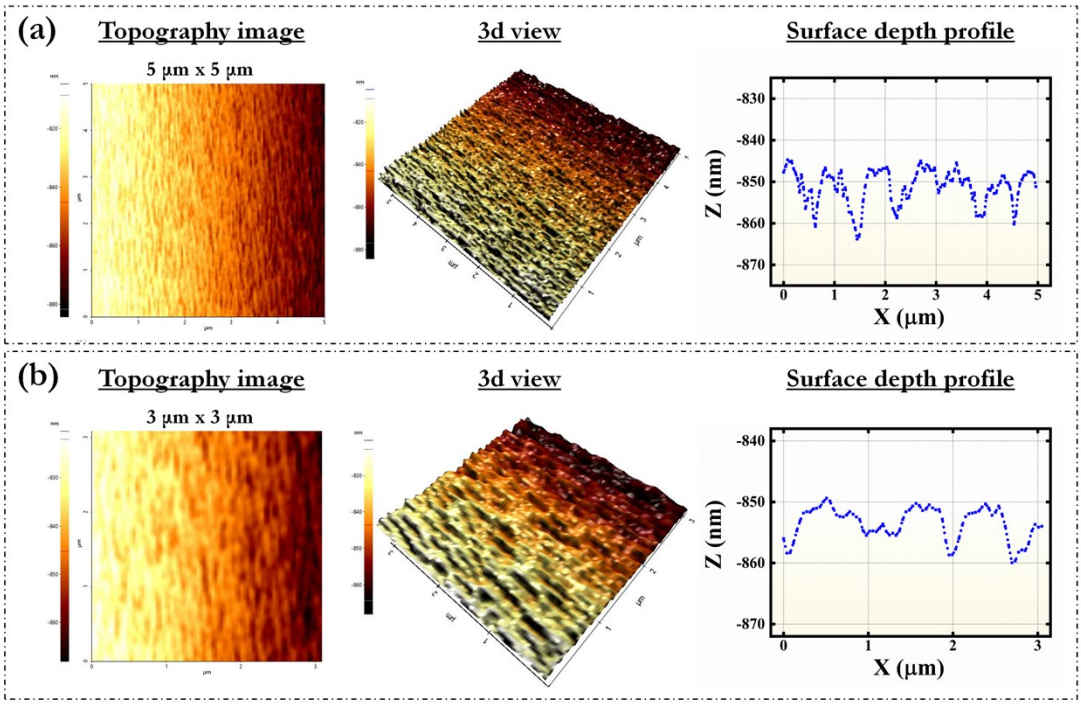

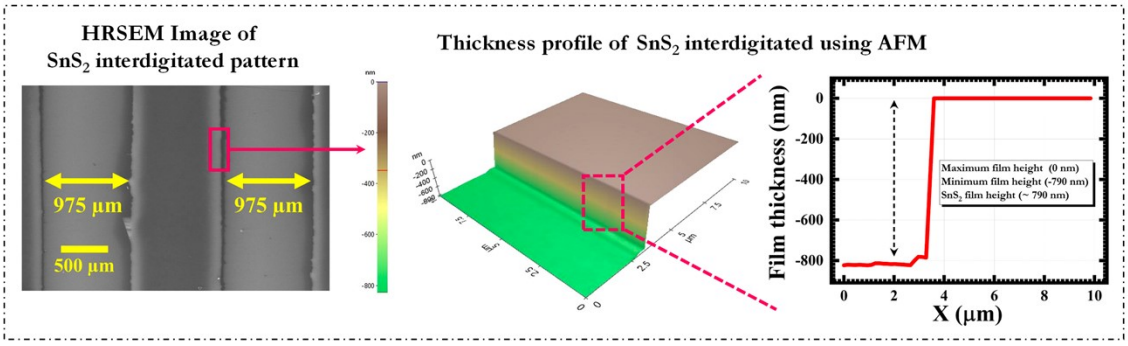

Fig. S2 (a and b) Topography and surface roughness at different magnification.

Fig. S3 HRSEM image of the SnS_2 interdigitated pattern, and Thickness profile of the SnS_2 interdigitated pattern using AFM technique.

ISC device voltage window optimization studies:

Fig 4a compares the CV curves for the ISC device, recorded various voltage ranges of 0-0.9 V, 0-1 V, 0-1.1 V and 0-1.2 V at a constant scan rate of 50 mV s^{-1}. Fig 4b, the GCD curves for the ISC device are shown, recorded various voltage ranges of 0-0.9 V, 0-1 V, 0-1.1 V and 0-1.2 V at a constant current density of 13.8 A cm^{-3}. Fig 4c indicates the calculated volumetric capacitance (C_{Vol}) values as a function of voltage from the CV study. In Fig 4d illustrates the calculated C_{Vol} and coulombic efficiency across various voltages. A pronounced drop in coulombic efficiency and onset of interfacial decomposition were observed at voltages exceeding 1.0 V. A pronounced reduction in coulombic efficiency and the onset of interfacial decomposition are observed at voltages exceeding 1.0 V. Accordingly, the ISC device's intrinsic electrochemical stability limits the safe operating potential window to 0-1.0 V, which is adopted for all subsequent measurements.

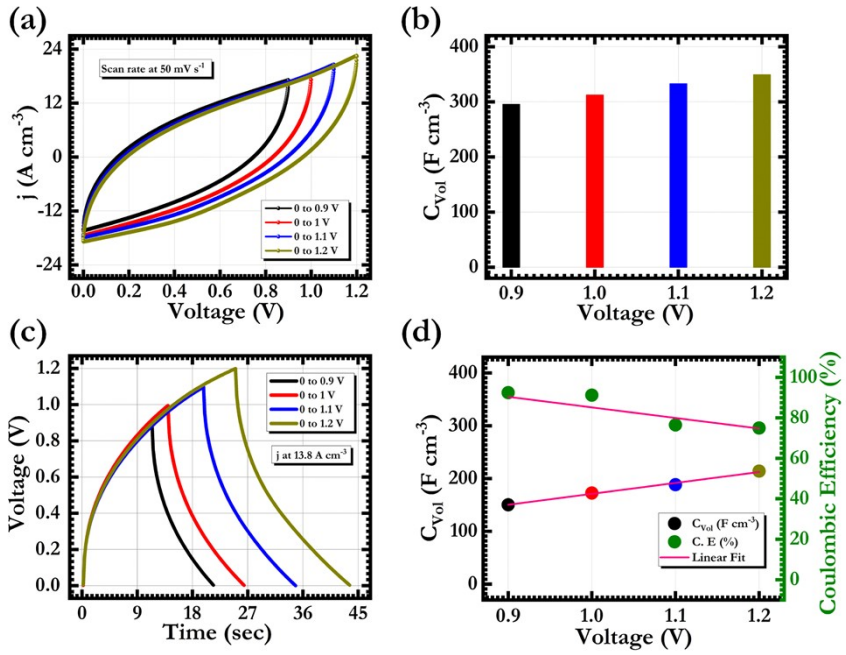

Fig. S4 (a) Voltage window optimization of ISC device at 50 mV s^{-1}, (b) Voltage window optimization of ISC device at 13.8 A cm^{-3}, (c) Voltage window dependent volumetric capacitance (C_{Vol}) from CV analysis, (d) Voltage window dependent volumetric capacitance (C_{Vol}) vs. coulombic efficiency from GCD analysis.

Areal Capacitance for ISC device:

Specific areal capacitance (C_{Areal}) values were determined for each scan rate using Equation S2, with a decrease in C_{Areal} observed at higher scan rates.

$$C_{Areal} = \frac{\oint i(t)dt}{Area \times \vartheta \times \Delta V} \quad \text{(S2)}$$

Here, ϑ and ΔV are the sweep rates and the voltage variation (1 V), i indicates measured current in CV, and t is time.

Table S1. Areal capacitance for ISC device

Scan rate (mV s^{-1})	C_{Areal} (mF cm^{-2})
5	92.8
10	63.3
25	34.3
50	22.0
75	17.1
100	14.5

ISC device cycle stability:

Electrochemical impedance spectroscopy (EIS) measurements were conducted prior to cycle stability testing, showing a resistance of 0.266 kΩ, which served as a reference for determining other cell properties (Fig. 5a). The initial ionic conductivity (σ_{AC}) was 6.981 x 10^{-4} S cm^{-1} (Fig. 5b), accompanied by a moderate dielectric response [ε (ω)] of 3.989 x 10^{4}. After 10000 cycles, the resistance increased slightly to 0.270 kΩ, while the dielectric response decreased marginally to 3.951 x 10^{4} and the ionic conductivity dropped to 6.910 x 10^{-4} S cm^{-1}. These variations confirm the decline in ionic conductivity and dielectric response for the ISC configuration upon cycling. The electron transfer rate constant (k_0) also showed a slight reduction, from 1.251 x 10^{-5} cm s^{-1} cm s^{-1} before cycling to 1.228 x 10^{-5} cm s^{-1} after 10000 cycles (Fig. 5c). Similarly, the diffusion coefficient (D_0) decreased from 3.852 x 10^{-11} cm^2 s^{-1} to 3.775 x 10^{-11} cm^2 s^{-1} (Fig. 5d). The kinetic analysis before and after cycling, incorporating parameters such as volumetric capacitance, ionic conductivity, electron transfer rate constant, diffusion coefficient, and carrier density, is summarized in Fig. 5e.

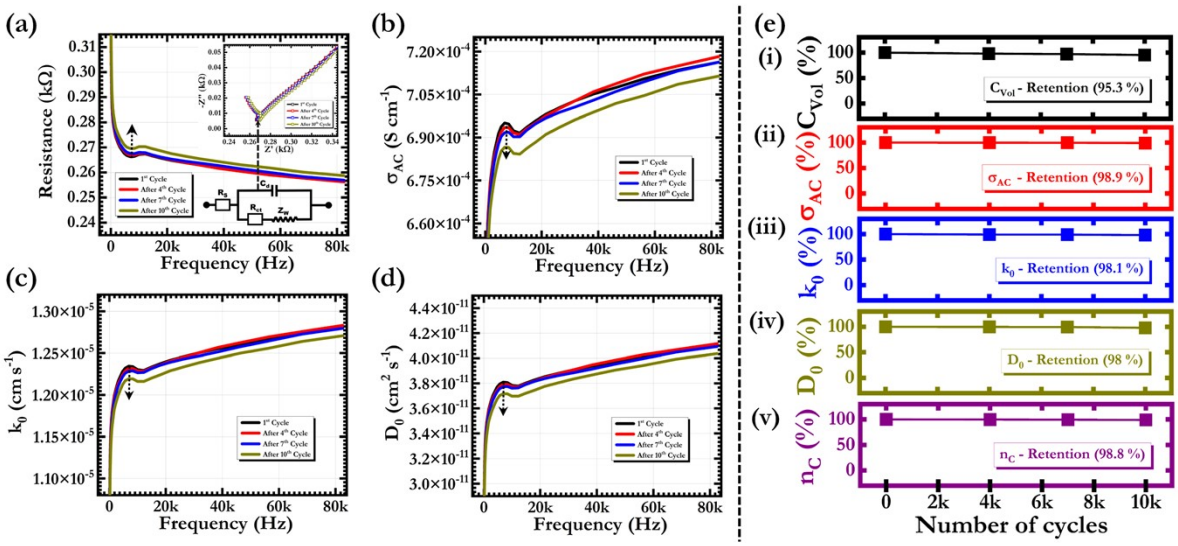

Fig. S5 (a) Comparison of Resistance/EIS spectra of before and after cycle stability (10000) studies, (b) Frequency vs. AC conductivity at before and after cycle stability studies, (c) Frequency vs. Electron transfer rate constant at before and after cycle stability studies, (d) Frequency vs. Diffusion coefficient at before and after cycle stability studies, (e) Stack graphs indicate the kinetic studies such as No of cycles vs. C_{Vol}, σ_{AC}, k_0, D_0, and n_C at before and after cycle stability studies.

No of cycle	C_{Vol} (F cm^{-3})	σ_{AC} (S cm^{-1})	k_0 (cm s^{-1})	ε (ω)	D_0 (cm^2 s^{-1})	n_c (cm^{-3})
1st Cycle	173.4	6.981 x 10^{-4}	1.251 x 10^{-5}	3.989 x 10^4	3.852 x 10^{-11}	3.570 x 10^{10}
After 4000	170.0	6.975 x 10^{-4}	1.240 x 10^{-5}	3.988 x 10^4	3.847 x 10^{-11}	3.563 x 10^{10}
After 7000	168.5	6.967 x 10^{-4}	1.239 x 10^{-5}	3.976 x 10^4	3.838 x 10^{-11}	3.557 x 10^{10}
After 10000	165.3	6.910 x 10^{-4}	1.228 x 10^{-5}	3.951 x 10^4	3.775 x 10^{-11}	3.536 x 10^{10}

Table S2. ISC device cycle life characteristics from EIS measurement

Table S3. Compare coulombic efficiency, Volumetric capacitance, energy density and power density for ISC device

Interdigitated super capacitors (ISC)				
Current (A)/ Current density (A cm^{-3})	**Coulombic Efficiency (%)**	**Volumetric capacitance, C_{Vol} (F cm^{-3})**	**Volumetric energy density (Wh cm^{-3})**	**Volumetric power density (W cm^{-3})**
0.000162/ 3.6	96.4	977.5	135.7	1.802
0.000189/ 4.2	95.4	867.7	120.5	2.128
0.000216/ 4.8	95.1	773.7	107.4	2.433
0.000243/ 5.4	94.6	681.0	94.5	2.737
0.000270/ 6.0	94.9	586.3	81.4	3.041
0.000324/ 7.2	95.2	435.0	60.4	3.649
0.000378/ 8.5	95.3	347.4	48.2	4.257
0.000434/ 9.9	96.8	301.1	41.8	4.888

156

157

158 **Table S4.** References mentioned in the above table.

Ref No	MSCs (Positrode ‖ Negatrode)	Fabrication method	Electrolyte	C_{Areal} (mF cm^{-2})	ED_{Areal} (µWh cm^{-2})	Cycle stability (%)
	SnS_2: ISC (This work)	**E- beam technique**	**PVA-$LiClO_4$**	92.8	**22.32**	**10000 (95.4%)**
1	rGO	Photolithography	PVA-H_2SO_4	0.95	-	11000 (98.3%)
2	$NiFe_2O_4$	Photolithography	PVA-KOH	0.067	0.006	10000 (93.6%)
3	C/CHIT-CNT	Photolithography	1M H_2SO_4	6.09	-	10000 (99.9%)
4	C/Sn QDs	Photolithography	PVA-H_2SO_4	5.79	-	5000 (93.3%)
5	MXene	Ink printing	PVA-H_2SO_4	27.29	-	-
6	EEG	Ink printing	PSSH	0.7	-	11000 (77%)
7	$Co(OH)_2$ ‖ VN	Ink printing	PVA-KOH	21	-	10000 (84%)
8	GO/PANI ‖ Graphene	Ink printing	PVA-H_3PO_4	153.6	15.4	5000 (100%)
9	MnO_2 ‖ Graphene	Ink printing	PVA-H_2SO_4	7.6	-	10000 (91.1%)
10	EG/PEDOT: PSS	Ink printing	PVA-H_2SO_4	5.4	-	5000 (90%)
11	MnO_2	Ink printing	PVA-$LiClO_4$	26.6	-	1000 (100%)
12	GCP	Ink printing	PVA-H_3PO_4	107.5	1.27	8000 (93.2%)
13	PG	Ink printing	PVA-H_2SO_4	9.8	-	2000 (89.5%)
14	Graphene	Screen printing	PVA-H_3PO_4	1.0	-	10000 (91.8%)
15	Graphene	Screen printing	PVA-H_3PO_4	5.2	0.06	2000 (89.5%)
16	Ag@PPy	Screen printing	PVA-H_3PO_4	47.5	-	10000 (82.6%)
17	MnO_2	Screen printing	1M Na_2SO_4	2.1	8.05	10000 (98.3%)

18	$Cu(OH)_2$@FeOOH	Screen printing	FS/EMIM-BF_4	58	18	10000 (82%)
19	rGO	Laser processing	PVA-H_3PO_4	15.3	-	10000 (94%)
20	rGO	Laser processing	PVA-LiCl	12.5	-	20000 (94.8%)
21	rGO	Laser processing	PVA-H_2SO_4	4.9	-	10000 (99%)
22	LIG	Laser processing	BMIM-BF_4	4	-	7000 (90%)
23	LIG	Laser processing	PVA-H_2SO_4	25.1	0.0026	12000 (99.2%)
24	B-doped LIG	Laser processing	PVA-H_2SO_4	16.5	-	12000 (90%)
25	CGF	Laser processing	PVA-H_3PO_4	1.7	0.22	1000 (89.4%)
26	WO_3/PVDF/MWCNT	Laser processing	PVA-H_3PO_4	62.4	-	2000 (80%)
27	MXene	Laser processing	PVA-H_2SO_4	27	-	10000 (100%)
28	Graphene	Plasma etching	PVA-H_2SO_4	116	-	50000 (98.5%)
29	EG/PANI	Plasma etching	1M H_2SO_4	1.5	-	1000 (94%)
30	MWCNT/AgNWs	Plasma etching	PVA-H_3PO_4	0.27	-	10000 (92.3%)
31	EG/PANI	Plasma etching	PVA-H_2SO_4	368	-	1000 (92.6%)
32	Graphene	Stamping	Ion gel	0.26	-	100000 (97%)
33	$Ti_3C_2T_X$	Stamping	PVA-H_2SO_4	61	0.76	10000 (94.1%)
34	MWCNT/PANI	Stamping	PMMA-PC-$LiClO_4$	44.1	0.004	20000 (87%)
35	Graphene	3D printing	PVA-H_2SO_4	58.7	-	10000 (100%)
36	LIG	Laser processing	PVA-H_2SO_4	31.9	-	3000 (98%)
37	LIG	Laser processing	PVA-H_3PO_4	2.31	-	100000 (100%)
38	MoS_2 doped LIG	Laser processing	PVA-H_2SO_4	16	-	5000 (92%)
39	$NiCo_2S_4$/CNF	Laser processing	1M KOH	4000	200	10000 (89%)

40	V_2O_5 ‖ G-VNQDs	3D printing	PVA-LiCl	207.9	73.9	8000 (65%)
41	PANI/rGO	3D printing	1M H_2SO_4	1329	-	1000 (75%)

Reproducibility of ISC Device Performance

To assess the reproducibility and stability of the fabricated ISC devices, cyclic voltammetry (CV) measurements were repeatedly performed on three independently prepared devices (Devices 1-3). Fig. 6a shows the CV characteristics of Devices 1-3 measured at a constant scan rate of 100 mV s^{-1}. All devices exhibit similar curve shapes and current responses, confirming high reproducibility across multiple samples. Fig. 6b presents the CV curves of Device 1 measured three consecutive times at 100 mV s^{-1}, showing nearly overlapping profiles and demonstrating excellent repeatability of the electrochemical response. Fig. 6c performances a comparative plot illustrating the reproducibility and repeatability of the capacitance for all three devices (Devices 1–3). Summarize the calculated mean capacitance ($\bar{C}$) of 136.1 F cm^{-3}, with a standard deviation, SD of 10.62 F cm^{-3} and an error of ±7.8 %, verifying consistent device fabrication and reliable measurement reproducibility (Figs. 6d-6f).

Additionally, the step-by-step calculations for mean capacitance ($\bar{C}$), standard deviation, and percentage error are also included for transparency and validation of the reproducibility results. [42]

(i) Mean Capacitance ($\bar{C}$): represents the average capacitance value from repeated measurements, showing the typical charge storage ability of the ISC device.

$$\bar{C} = \frac{1}{n}\sum_{i=1}^{n} C_i \qquad \text{(S3)}$$

where $\bar{C}$ means (average) capacitance (F cm^{-3}), C_i means individual capacitance value (F cm^{-3}) from each measurement, and n means total number of measurements.

(ii) Standard deviation, SD: Indicates how much the measured capacitance values deviate from the mean a smaller value means higher reproducibility.

$$SD = \sqrt{\frac{\sum_{i=1}^{n}(C_i - \bar{C})^2}{n-1}} \quad \text{(S4)}$$

where s means standard deviation, C_i means individual capacitance value (F cm^{-3}) from each measurement, $\bar{C}$ means capacitance (F cm^{-3}), and n means total number of measurements.

(iii) percentage error (%): expresses the variation as a percentage of the mean, showing the precision or consistency of the measurements.

$$Error\ (\%) = \frac{SD}{\bar{C}} \times 100 \quad \text{(S5)}$$

where s means standard deviation,

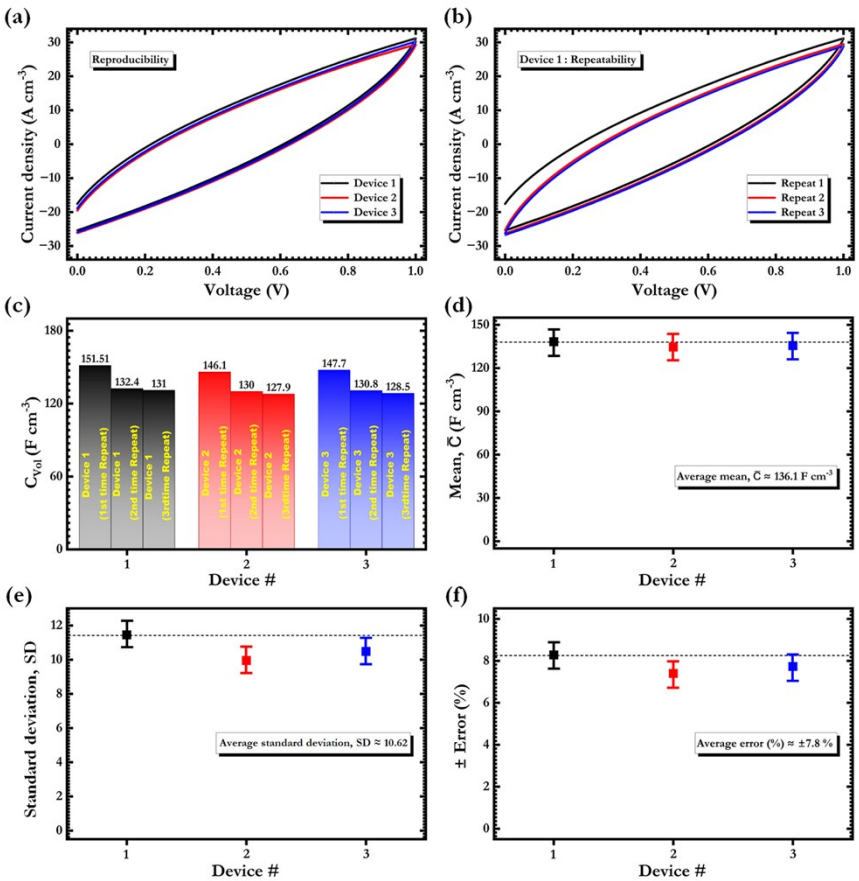

$\bar{C}$ means capacitance (F cm^{-3}).

Fig. S6 (a) CV studies of three different ISC devices (Devices 1-3) measured at a constant scan rate of 100 mV s^{-1} (b) CV curves of Device 1 measured three consecutive times at 100 mV s^{-1}, (c) reproducibility and repeatability of the capacitance for all three devices, (d) mean capacitance for all three devices, (e and f) Statistical comparison of standard deviation and error % for all three devices.

Table S5. Reproducibility of Mean capacitance (C), standard deviation, SD, and error (%) for three ISC devices (1-3)

Device #	Mean capacitance, $\overline{C}$ (F cm^{-3})	Standard deviation, SD	Error (%)
Device 1	138.3	11.45	±8.28
Device 2	134.6	9.95	±7.4
Device 3	135.6	10.48	±7.73
Average	136.1	10.62	±7.8

230 **Kinetic** **study**

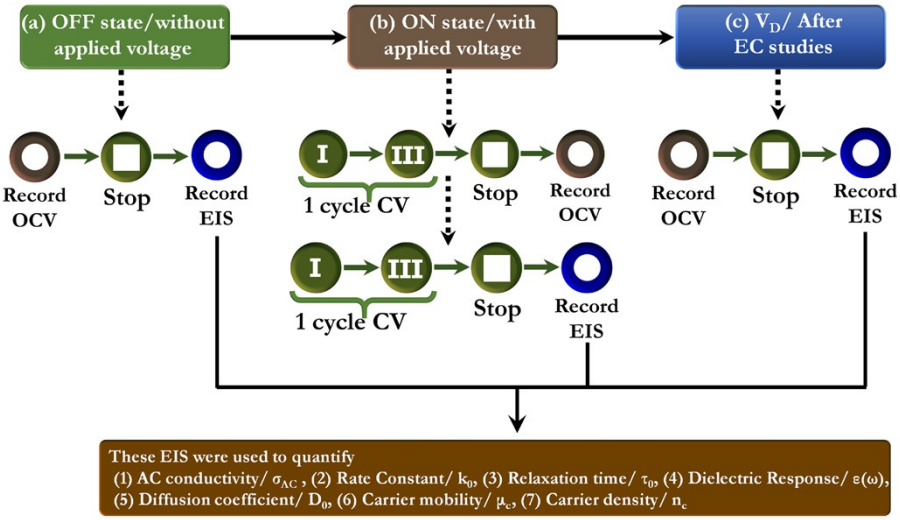

232 **measurements**

233

234

235

236

237

238

239

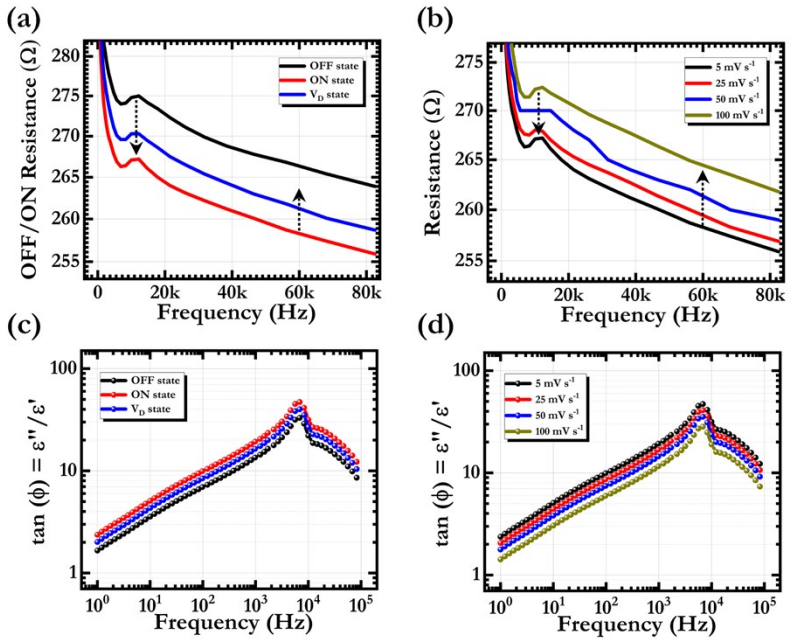

240 **Fig. S7** (a-c) Flow chart

241 of OFF, ON and VD

242 state Switching

243 studies.

244 **Resistance** **operation**

and tangent loss for ISC device

Fig. S8 (a and b) resistance operation under various device state and various sweep rate, (c and d) tan loss under various device state and various sweep rate.

Proposed interface switching mechanism at various sweep rates:

Furthermore, a time-dependent voltage study was conducted under bias conditions following

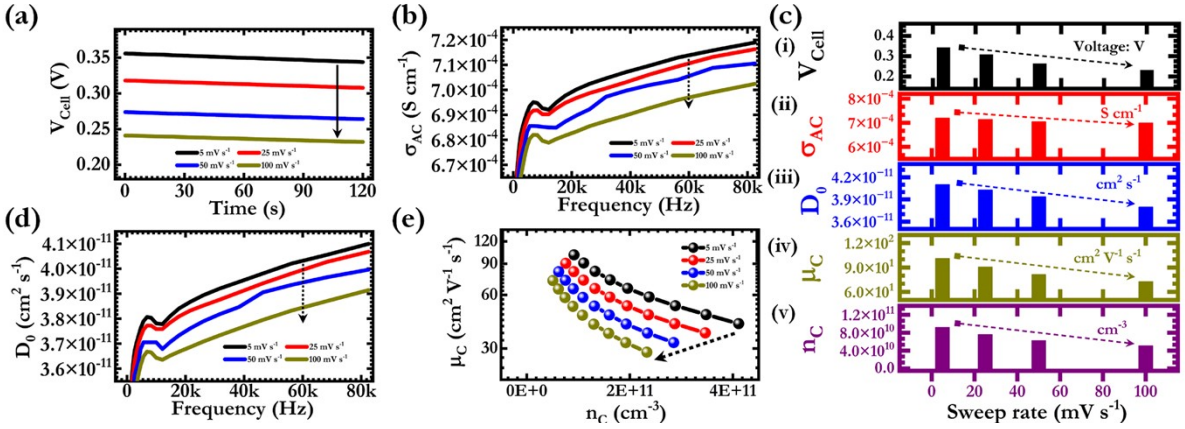

one cycle of CV at different sweep rates

Fig. S9 (a) Time dependent cell voltage (V_{Cell}) under various sweep rate: 5 – 100 mV s^{-1} for ISC configuration, (b, d, e) Operational frequency dependent σ_{AC}, D_0, μ_c, and n_c across various sweep rate, (c) stack plots comparing kinetic parameters (V_{Cell}, σ_{AC}, D_0, μ_c, and n_c) across various sweep rate.

Table S6. Quantification of the cell characteristics from EIS measurements for interdigitated (ISC) device under various sweep rates.

Sweep rate (mV s^{-1})	V_{Cell} (V)	σ_{AC} (S cm^{-1})	k_0 (cm s^{-1})	DER ε (ω)	D_0 (cm^2 s^{-1})	μ_c (cm^2 V^{-1} s^{-1})	n_c (cm^{-3})
5	0.343	7.189×10^{-4}	1.280×10^{-5}	7.052×10^{4}	4.099×10^{-11}	100.92	9.162×10^{10}
25	0.309	7.132×10^{-4}	1.269×10^{-4}	5.831×10^{4}	4.027×10^{-11}	90.42	7.575×10^{10}
50	0.265	7.040×10^{-4}	1.254×10^{-4}	4.772×10^{4}	3.935×10^{-11}	81.07	6.199×10^{10}
100	0.233	6.926×10^{-4}	1.232×10^{-4}	3.902×10^{4}	3.795×10^{-11}	72.33	5.069×10^{10}

Electron transfer rate constant (k_0) at various device state, various sweep rate operation for ISC device

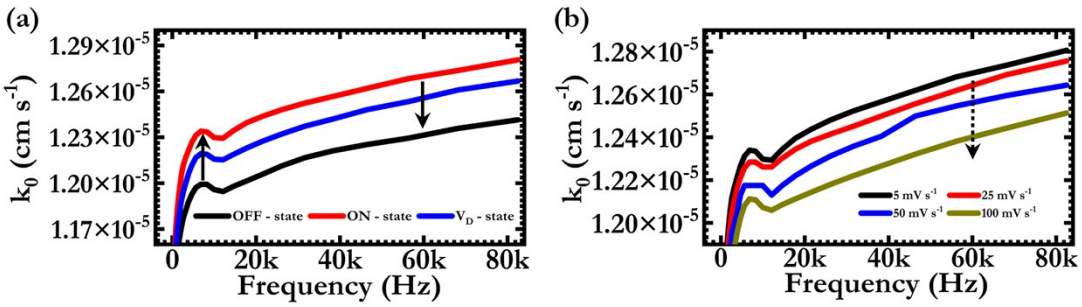

Fig. S10 (a and b) kinetic studies such as Frequency vs. k_0 under various device states and various sweep rates for ISC device.

Specifically, included worked-out steps for the OFF-state of the ISC device, based on the Kramers-Kronig relations, showing how ε'(ω) and ε"(ω) were numerically obtained from the impedance data using the trapezoidal rule.

(i) $$\varepsilon'(\omega) = R_\infty + \frac{2}{\pi}\int_0^\infty \left(\frac{xZ''(x) - \omega Z''(\omega)}{x^2 - \omega^2}\right)dx$$

We approximate the integral using the trapezoidal rule,

$$= \sum_{i=1}^{N-1} \frac{[(xZ''(x) - \omega Z''(\omega)) + (x_{i+1}Z''(x_{i+1}) - \omega Z''(\omega))]}{(x+\omega)*(x-\omega)} \times \frac{(x_{i+1} - x_i)}{2}$$

expression is equal to $\approx \dfrac{Z''}{\omega C_o(Z'^2 + Z''^2)}$ (S6)

(ii) $$\varepsilon''(\omega) = \frac{2}{\pi}\int_0^\infty \left(\frac{Z'(x) - Z'(\omega)}{x^2 - \omega^2}\right)dx$$

We approximate the integral using the trapezoidal rule,

$$= \sum_{i=1}^{N-1} \frac{[(xZ'(x) - \omega Z'(\omega)) + (x_{i+1}Z'(x_{i+1}) - \omega Z'(\omega))]}{(x+\omega)*(x-\omega)} \times \frac{(x_{i+1} - x_i)}{2}$$

expression is equal to $\approx \frac{Z'}{\omega C_o(Z'^2 + Z''^2)}$ (S7)

P-S circuits	C_{Vol} (F cm^{-3})	σ_{AC} (S cm^{-1})	k_0 (cm s^{-1})	DER	D_0 (cm^2 s^{-1})	μ_c (cm^2 V^{-1} s^{-1})	n_c (cm^{-3})
4 P circuit	1770.8	1.946 x 10^{-3}	3.456 x 10^{-5}	7.787 x 10^{4}	2.986 x 10^{-10}	124.20	1.011 x 10^{11}
1 P/S circuit	771.2	6.788 x 10^{-4}	1.205 x 10^{-5}	2.672 x 10^{4}	3.635 x 10^{-11}	65.11	3.472 x 10^{10}
4 S circuit	587.2	2.468 x 10^{-4}	4.388 x 10^{-6}	9.690 x 10^{3}	4.815 x 10^{-12}	38.03	8.655 x 10^{9}

$$\varepsilon(\omega) \approx \left\{ R_\infty + \frac{2}{\pi}\int_0^\infty (Z'(x) - Z'(\omega)) dx \right\} + \frac{2}{\pi}\int_0^\infty (xZ'(x) - \omega Z''(\omega))$$

$$implies tan(\phi) = \frac{(S7)}{(S6)}$$ equations

Electrochemical performances comparison of parallel- series (P-S) connection for ISC

Table S7. Comparison of kinetic studies for the 4 P, 1 P/S, and 4 S circuit.

Charge storage mechanism:

According to Dunn's equation (eqn. S8), the current response (i_p) at a given potential follows a power law related to the scan rate (ϑ), where both a and b are limitation parameters. The coefficient b is derived from the slope of the log(ip) versus log(ϑ) plot (Fig 11a). The relationship between the scan rate (ϑ) and current (A) is utilized to identify the b coefficient. The benchmarks b = 0.5 and b = 1.0 indicate diffusion-limited and capacitive responses, respectively.

$$i_p = a\vartheta^b \quad \text{(S8)}$$

When b = 0.5, the current response is predominantly diffusion-limited, described by eqn. S9.

$$i_p = nFAC_o^* D_o^{1/2} \vartheta^{1/2} (\alpha nF/RT)^{1/2} \pi^{1/2} \chi(bt) \quad \text{(S9)}$$

In this equation, C_0^* represents the concentration of the electrode material, D_0 is the chemical diffusion coefficient, and the χ (bt) function denotes the regularized current for a fully irreversible system, as suggested by the cyclic voltammetry response. The variables include, n is the number of electrons involved in the electrode reaction, A is the surface area of the electrode material, F is the Faraday constant, R is molar gas constant, α is transfer coefficient, π is circumstance of a circle, and T is absolute temperature.

When b = 1.0, the current is predominantly capacitive and proportional to the scan rate.

$$i_p = \vartheta AC \quad \text{(S10)}$$

where C means capacitance. A value of 0.5 < b < 1.0 indicates a transition between diffusion-controlled and capacitive charge storage processes (eqn. S10).

Equation. S11 differentiates the current response at a fixed potential into diffusion-controlled and capacitive components (Fig 11b and 11c).

$$i_P = k_1 \vartheta + k_2 \sqrt{\vartheta} \quad \text{(S11)}$$

The term $k_1\vartheta$ represents the capacitive current, while $k_2\sqrt{\vartheta}$ denotes the diffusion-limited current,

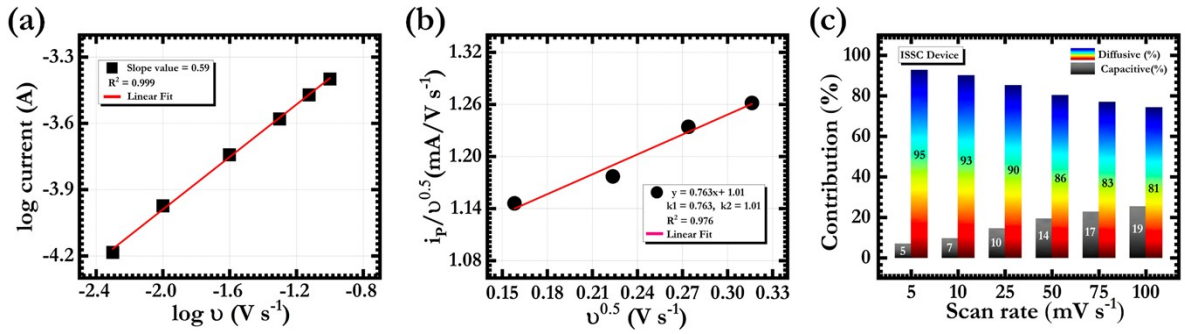

where k_1 and k_2 are constants.

Fig. S11 (a) b-coefficient value for ISC devices, (b) Calculation of diffusive and capacitive behavior by plotting $\sqrt{\vartheta}$ vs. $i_p/\sqrt{\vartheta}$, (c) Contribution percentage.

Flexibility demonstration for ISC devices

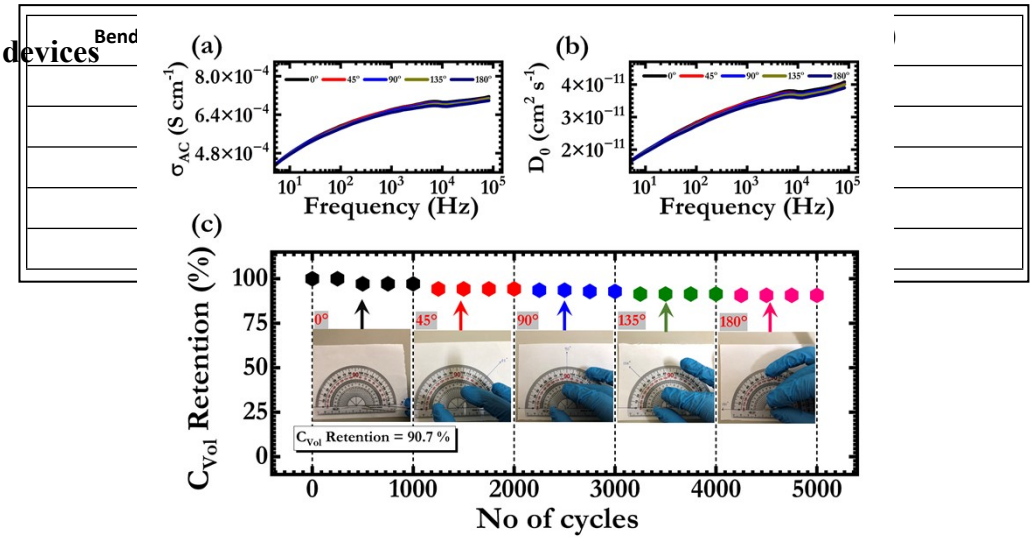

Fig. S12 (a and b) Frequency dependent σ_{AC}, and D_0 at bending angles, (c) cyclic stability under various bending angles.

Table S8. Flexibility demonstration experimental values for ISC device.

References:

1. Z.-K. Wu, Z. Lin, L. Li, B. Song, K.-S. Moon, S.-L. Bai, C.-P. Wong, *Nano Energy,* **2014**, *10*, 222.
2. L. Li, Z. Lou, W. Han, G. Shen, *Nanoscale* **2016**, *8*, 14986.
3. Y. Yang, L. He, C. Tang, P. Hu, X. Hong, M. Yan, Y. Dong, X. Tian, Q. Wei, L. Mai, *Nano Res*. **2016**, *9*, 2510.
4. X. Hong, L. He, X. Ma, W. Yang, Y. Chen, L. Zhang, H. Yan, Z. Li, L. Mai, *Nano Res*. **2017**, *10*, 3743.
5. H. Hu, T. Hua, *J. Mater. Chem. A* **2017**, *5*, 19639.
6. J. Li, S. S. Delekta, P. Zhang, S. Yang, M. R. Lohe, X. Zhuang, X. Feng, M. Ostling, *ACS Nano* **2017**, *11*, 8249.
7. S. Wang, Z. S. Wu, F. Zhou, X. Shi, S. Zheng, J. Qin, H. Xiao, C. Sun, X. Bao, *2D Mater. Appl.* **2018**, *2*, 7.
8. Y. Liu, B. Zhang, Q. Xu, Y. Hou, S. Seyedin, S. Qin, G. G. Wallace, S. Beirne, J. M. Razal, J. Chen, *Adv. Funct. Mater.* **2018**, *28*, 1706592.
9. X. Shi, Z. S. Wu, J. Qin, S. Zheng, S. Wang, F. Zhou, C. Sun, X. Bao, *Adv. Mater.* **2017**, *29*, 1703034.
10. Z. Liu, Z. S. Wu, S. Yang, R. Dong, X. Feng, K. Mullen, *Adv. Mater.* **2016**, *28*, 2217.
11. K. Guo, Y. Wan, N. Yu, L. Hu, T. Zhai, H. Li, *Energy Storage Mater.* **2018**, *11*, 144.

12. H. Xiao, Z.-S. Wu, F. Zhou, S. Zheng, D. Sui, Y. Chen, X. Bao, *Energy Storage Mater.* **2018**, 13, 233.

13. H. Xiao, Z. S. Wu, L. Chen, F. Zhou, S. Zheng, W. Ren, H. M. Cheng, X. Bao, *ACS Nano*. **2017**, 11, 7284.

14. X. Shi, S. Pei, F. Zhou, W. Ren, H. M. Cheng, Z. S. Wu, X. Bao, *Energy Environ. Sci.* **2019**, 12, 1534.

15. S. Bellani, E. Petroni, A. E. Del Rio Castillo, N. Curreli, B. Martin-Garcia, R. Oropesa-Nunez, M. Prato, F. Bonaccorso, *Adv. Funct. Mater.* **2019**, *29*, 1807659.

16. L. Liu, Q. Lu, S. Yang, J. Guo, Q. Tian, W. Yao, Z. Guo, V. A. L. Roy, W. Wu, *Adv. Mater. Technol.* **2018**, 3, 1700206.

17. R. Guo, J. Chen, B. Yang, L. Liu, L. Su, B. Shen, X. Yan, *Adv. Funct. Mater.* **2017**, 27, 1702394.

18. J.-Q. Xie, Y.-Q. Ji, J.-H. Kang, J.-L. Sheng, D.-S. Mao, X.-Z. Fu, R. Sun, C.-P. Wong, *Energy Environ. Sci.* **2019**, 12, 194.

19. M. Wu, Y. Li, B. Yao, J. Chen, C. Li, G. Shi, *J. Mater. Chem. A* **2016**, *4*, 16213.

20. Y. Chen, B. Xu, J. Xu, J. Wen, T. Hua, C.-W. Kan, *J. Power Sources.* **2019**, 420, 82.

21. R. Z. Li, R. Peng, K. D. Kihm, S. Bai, D. Bridges, U. Tumuluri, Z. Wu, T. Zhang, G. Compagnini, Z. Feng, A. Hu, *Energy Environ. Sci.* **2016**, 9, 1458.

22. J. Lin, Z. W. Peng, Y. Y. Liu, F. Ruiz-Zepeda, R. Q. Ye, E. L. G. Samuel, M. J. Yacaman, B. I. Yakobson, J. M. Tour, *Nat. Commun.* **2014**, 5, 5714.

23. W. Zhang, Y. Lei, F. Ming, Q. Jiang, P. M. Costa, H. N. Alshareef, *Adv. Energy Mater.* **2018**, 8, 1801840.

24. Z. Peng, R. Ye, J. A. Mann, D. Zakhidov, Y. Li, P. R. Smalley, J. Lin, J. M. Tour, *ACS Nano*. **2015**, 9, 5868.

25. Y. Shao, J. Li, Y. Li, H. Wang, Q. Zhang, R. B. Kaner, *Mater. Horiz.* **2017**, 4, 1145.

26. X. Huang, H. Liu, X. Zhang, H. Jiang, *ACS Appl. Mater. Interfaces.* **2015**, 7, 27845.

27. Y.-Y. Peng, B. Akuzum, N. Kurra, M.-Q. Zhao, M. Alhabeb, B. Anasori, E. C. Kumbur, H. N. Alshareef, M.-D. Ger, Y. Gogotsi, *Energy Environ. Sci.* **2016**, 9, 2847.

28. Z.-S. Wu, K. Parvez, X. Feng, K. Mullen, *J. Mater. Chem. A.* **2014**, *2*, 8288.

29. Z. Liu, S. Liu, R. Dong, S. Yang, H. Lu, A. Narita, X. Feng, K. Mullen, *Small.* **2017**, 13, 1603388.

30. L. Liu, H. Y. Li, Y. Yu, L. Liu, Y. Wu, *Nanotechnology.* **2018**, 29, 055401.

31. Z. S. Wu, K. Parvez, S. Li, S. Yang, Z. Liu, S. Liu, X. Feng, K. Mullen, *Adv. Mater.* **2015**, 27, 4054.

32. W. J. Hyun, E. B. Secor, C.-H. Kim, M. C. Hersam, L. F. Francis, C. D. Frisbie, Adv. *Energy Mater.* **2017**, 7, 1700285.

33. C. J. Zhang, M. P. Kremer, A. Seral-Ascaso, S.-H. Park, N. McEvoy, B. Anasori, Y. Gogotsi, V. Nicolosi, *Adv. Funct. Mater.* **2018**, 28, 1705506.

34. L. Li, Z. Lou, W. Han, D. Chen, K. Jiang, G. Shen, *Adv. Mater. Technol.* **2017**, 2, 1600282.

35. W. Li, Y. Li, M. Su, B. An, J. Liu, D. Su, L. Li, F. Li, Y. Song, *J. Mater. Chem. A.* **2017**, 5, 16281.

36. J. Cai, C. Lv, A. Watanabe, *J. Mater. Chem. A.* **2016**, 4, 1671.

37. N. Kamboj, T. Purkait, M. Das, S. Sarkar, K. S. Hazra, R. S. Dey, *Energy Environ. Sci.* **2019**, 12, 2507.

399 38. S. Wang, Y. Yu, S. Luo, X. Cheng, G. Feng, Y. Zhang, Z. Wu, G. Compagnini, J. Pooran, A. Hu,
400 *Appl. Phys. Lett.* **2019**, 115, 083904.
401 39. Q. Jiang, N. Kurra, C. Xia, H. N. Alshareef, *Adv. Energy Mater.* **2017**, 7, 1601257.
402 40. K. Shen, J. Ding, S. Yang, *Adv. Energy Mater.* **2018**, 8, 1800408.
403 41. Z. Wang, Q. E. Zhang, S. Long, Y. Luo, P. Yu, Z. Tan, J. Bai, B. Qu, Y. Yang, J. Shi, H. Zhou, Z.
404 Y. Xiao, W. Hong, H. Bai, *ACS Appl. Mater. Interfaces.* **2018**, 10, 10437.
405 42. S. Mishra, R. Srivastava, A. Muhammad, A. Amit, E. Chiavazzo, M. Fasano, P. Asinari, *Scientific*
406 *Reports*, **2023**, 13, 6494**.**